Journal of Marine Science and Technology

Volume 27 | Issue 5 Article 1

# On Waves Propagating Through an Emergent Poroelastic Medium

Yuan-Jyh Lan



Recommended Citation
Lan, Yuan-Jyh (2019) "On Waves Propagating Through an Emergent Poroelastic Medium," *Journal of Marine Science and Technology*: Vol. 27: Iss. 5, Article 1.
DOI: 10.6119/JMST.201910_27(5).0001
Available at: https://jmstt.ntou.edu.tw/journal/vol27/iss5/1

# On Waves Propagating Through an Emergent Poroelastic Medium

## Acknowledgements

This research was financially supported by the Ministry of Science and Technology, Taiwan, under grant no. MOST 106-2221-E-019-034.

*Journal of Marine Science and Technology, Vol. 27, No. 5, pp. 377-391 (2019)*
DOI: 10.6119/JMST.201910_27(5).0001


# ON WAVES PROPAGATING THROUGH AN EMERGENT POROELASTIC MEDIUM

Yuan-Jyh Lan

Key words: waves, poroelastic medium, interaction.

## ABSTRACT

This paper describes a theoretical study of the problem of linear waves propagating over an emergent poroelastic medium. Lan-Lee's poro-elastomer theory is extended to derive a new analytical solution for describing this problem, with the free surface boundary condition discussed in the context of a poroelastic medium, a topic that has rarely been covered by previous studies. In the present approach, the problem domain is divided into three subregions and a negligible water-exposed region. Using general solutions for each region and the matching dynamic and kinematic conditions for neighboring regions, a set of simultaneous equations is developed and numerically solved. The present analytic solution compares reasonably well with simplified cases of impermeable, rigid structures and porous structures. Using this analytic solution, the wave reflection and transmission induced by different key parameters of the poroelastic medium are studied. The results show that softer poroelastic media can transform the incident waves. For almost impermeable conditions, a softer emergent medium induces resonance, whereas higher permeability depresses the resonant effects and induces significant wave damping.

## I. INTRODUCTION

In recent years, fears about global climate change impacting extreme weather events and rising sea levels have led to increased interest in nonintrusive forms of shore protection such as vegetation. Such schemes are intended to protect the shoreline and provide a natural habitat for many different species of fish, amphibians, shellfish, insects, and birds (Augustin et al., 2009). Using near-natural and ecological coastal engineering increases the demands on structures and construction methods, as they no longer have the simple purpose of defense. Not only should the construction methods accommodate the natural environment, but various structural materials from local environments should also be used (Lan et al., 2013). Various novel wave-defense structures can use flexible materials such as rubber-dams, multi-material composite breakwaters, and flora, instead of the rigid materials of concrete and block stone, to reduce the wave energy transferred to the shoreline. The flexibility of soft materials means that the deformation induced by water waves disturbs the flow field in the vicinity of the structure, particularly when compared with their impermeable reflective concrete counterparts. For the wave attenuation effect caused by the permeable structures, different structural material properties have different wave damping characteristics, such as the flow configurations of Darcy, Darcy-Forchheimer and vegetation drag resistance, etc. Therefore, in academic and practical studies, near-natural and ecological wave-defense structures need to consider both the flexibility and permeability of the material composition, such as the poroelastic type. This paper theoretically investigates the additional flexible effect of permeable media on wave scattering and energy dissipation.

The fundamental research on wave propagation through poroelastic media mainly includes two major categories: seismic wave and gravity water wave. Seismic waves are divided into body waves transmitted inside the medium (including P waves and S waves) and surface waves transmitted on the surface of the medium (including Rayleigh waves, Love waves, Stoneley waves, etc.). Related researches focus on the conduction velocity and attenuation of seismic waves in poroelastic/poroviscoelastic viscoelastic media containing homogeneity/mesoscopic inhomogeneity (Liu, 2009; Liu et al., 2011; Zhang et al., 2014; Tcheverda et al., 2017; Tong et al., 2017; Xie and Yang, 2018). Various studies on interactions between gravity water waves and flexible media have considered flexible structures (Watarai et al., 1987; Lee and Chen, 1990; Lee and Lan, 1991), flexible and porous breakwaters (Wang and Ren, 1993; Yip et al., 2002; Shanta and Sahoo, 2006; Mandal and Sahoo, 2014), elastic membranes and air balloons (Chou and Fang, 1995; Sawaragi, 1995), submerged flexible mounds and reefs (Ohyama et al., 1989; Lan and Lee, 2010; Lan et al., 2011; 2013; 2016), and aquatic vegetation fields (Möller et al., 1999; Mendez and Losada, 2004; Li and Yan, 2007; Augustin et al., 2009; Stratigaki et al., 2011; Jadhav et al., 2013; John et al.,

*Paper submitted 12/19/18; revised 02/12/19; accepted 06/18/19. Author for correspondence: Yuan-Jyh Lan (e-mail: yjlan@mail.ntou.edu.tw).*
*Center of Excellences for the Oceans, National Taiwan Ocean University, Keelung, Taiwan, R.O.C.*

2015). The complex dynamic mechanisms in poroelastic media complicate the study of wave interactions with poroelastic structures. The problem of waves propagating over poro-elastomers involves analyses of wave motion, the dynamic behavior of poroelastic media, the interaction between waves and elastomers, and the fluid flux inside the poroelastic media (Lan and Lee, 2010). Biot's theory (1956) has often been used to describe the behavior of poroelastic media for waves propagating over flexible and permeable structures. The flow inside the porous media obeys Darcy's seabed law, the Darcy-Forchheimer (high permeability with turbulent resistance) relation, or is affected by vegetation. Related investigations have examined a poroelastic seabed of infinite width (Chen et al., 1997; Tseng et al., 2008) as well as flexible and permeable plates or breakwaters (Wang and Ren, 1993; Yip et al., 2002). These studies employed a simplified formulation in which the unlimited width of the bed and particular structural size ensured no changes along the horizontal direction and the thin poroelastic plates reduced the complexity of the flexible and permeable mechanisms. For finite-size homogeneous structures, Lan and Lee (2010) improved Biot's theory for the evaluation of Darcy-Forchheimer permeable resistance introduced by Sollitt and Cross (1972). They analyzed the reflection, transmission, and energy dissipation of regular waves passing over a single rectangular submerged poroelastic breakwater. Since the submerged medium does not encounter the free surface boundary, Lan-Lee's poro-elastomer theory ignored the static pore pressure. Based on the work of Lan and Lee (2010), the studies on waves interaction with poroelastic submerged media have considered a series of soft reefs (Lan et al., 2011), the adjoining-type composite breakwaters (Lan et al., 2013), and the mound-type composite structures (Lan et al., 2016). Among them, Lan et al. (2011) verified the rationality of Lan-Lee's poro-elastomer theory in the case of poroelastic media by conducting an experiment on a series of soft permeable breakwaters. Li and Yan (2007) proposed a fully three-dimensional numerical model in which the Reynolds-averaged Navier-Stokes equations simulate the wave-current-vegetation interaction phenomena. Based on the Biot theory, Tong et al. (2017) studied the propagation of nonlinear waves in porous media by introducing three new nonlinear parameters to consider the coupled nonlinearity between the solid and fluid components in porous media.

In this study, as an extension of Lan-Lee's poro-elastomer theory (Lan and Lee, 2010) and consideration of the static pore pressure, an analytical solution is obtained for wave scattering by an emergent poroelastic medium. The study deals with the free surface boundary condition in the field of poroelastic medium that previous studies have paid less attention. A partition method is employed and the solution is given in terms of orthogonal eigenfunctions. The matching conditions of the pore pressure and normal flow flux, as well as the continuity of both the medium displacements and stresses, are imposed on the interface boundaries. This solution provides a general and economical approach for investigating the wave scattering and energy dissipation over a pseudo-natural structure without extensive experimentation. Various parameters are analyzed to account for the reflection and transmission coefficients. The results calculated from the analytical solution are compared with previous results, and the key features of wave transformation induced by various shear moduli and permeable coefficients are discussed.

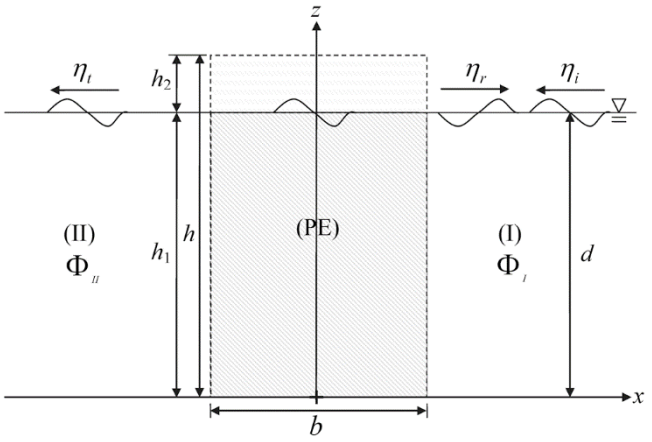


**Fig. 1. Sketch of boundary value problem of waves passing an emergent poroelastic medium.**

## II. PROBLEM FORMULATION

An emergent poroelastic medium with a rectangular shape is fixed on an impermeable seabed, and is subjected to incident waves. The poroelastic medium is assumed to be homogeneous, isotropic, and elastic. A schematic of this formulation is illustrated in Fig. 1, where $d$ is the water depth, $h$ and $b$ are the height and width of the poroelastic medium, $h_1 + h_2 = h$, and $h_1 = d$. A two-dimensional Cartesian coordinate system is used, with the origin located at the interface between the impermeable seabed surface and the center of the poroelastic medium, the $x$-axis pointing to the right, and the $z$-axis pointing upward. Incident waves propagate in the negative $x$ direction. The wave profile $\eta_i$ and velocity potential function $\Phi^i$ can be expressed as

$$\eta_i = \mathrm{Re}\left\{ \frac{H_i}{2} e^{-ik_0\left(x-\frac{b}{2}\right)} e^{-i\omega t} \right\} \tag{1}$$

$$\Phi^i = -i\frac{g H_i}{2\omega}\frac{\cosh k_0 z}{\cosh k_0 d}\, e^{-ik_0\left(x-\frac{b}{2}\right)} e^{-i\omega t} \tag{2}$$

where $\mathrm{Re}\{\ \}$ is the real part of a complex variable, $H_i$ is the incident wave height, $k_0$ is the wavenumber, $\omega = 2\pi/T$ is the angular frequency, $T$ is the wave period, $t$ denotes time, $g$ is gravitational acceleration, and $i = \sqrt{-1}$ is the complex unit.

To solve this problem, the study domain is divided into two fluid regions (regions I and II) and a poroelastic (PE) region, as shown in Fig. 1. The kinematic and dynamic effects of the exposed water part of the poro-elastomer are ignored.

## 1. Governing Equations for Poroelastic Media

The poroelastic medium in the PE region is assumed to be homogeneous, isotropic, and saturated with poroelastic features. In this situation, the governing equations for the poroelastic medium field are satisfied three decoupled partial differential equations (PDEs) in components of displacement in the $x$- and $z$-directions ($\xi$, $\chi$), and the pore pressure ($P$) as follows:

$$\left\{[\nabla^2+\alpha_1{}^2]\nabla^2+\alpha_2{}^4\right\}(\nabla^2+\alpha_3{}^2)\begin{Bmatrix}\xi\\ \chi\end{Bmatrix}=0 \tag{3}$$

$$\left\{[\nabla^2+\alpha_1{}^2]\nabla^2+\alpha_2{}^4\right\}P=0 \tag{4}$$

The coefficients $\alpha_1$, $\alpha_2$, and $\alpha_3$ are given by:

$$\alpha_1{}^2=\omega^2\rho_w\beta(S+if_p)+\frac{1-2\mu}{2G(1-\mu)}(\omega^2)\left\{\bar{\rho}+\rho_w\left[\frac{(S+if_p)}{n'}-2\right]\right\} \tag{5}$$

$$\alpha_2{}^4=\frac{1-2\mu}{2G(1-\mu)}(\omega^4\rho_w\beta)\,[\bar{\rho}(S+if_p)-n'\rho_w] \tag{6}$$

$$\alpha_3{}^2=\frac{\omega^2}{G}\left(\bar{\rho}-\frac{n'\rho_w}{(S+if_p)}\right) \tag{7}$$

where $\rho_w$ is the density of the fluid, $n'$ is the porosity of the poroelastic medium, $\beta$ is the compressibility of the pore fluid, $\bar{\rho}=(1-n')\rho_s+n'\rho_w$ is the mean density of the poroelastic medium, $\rho_s$ is the density of the elastic solid structure, $G=E/[2(1+\mu)]$ is the shear modulus, $E$ is Young's modulus, $\mu$ is Poisson's ratio, $S$ is the virtual mass coefficient, and $f_p$ is the linear friction factor. The form of Eqs. (3) and (4) is the same as that proposed by Lan and Lee (2010). In addition, note that the relative velocity $\vec{\boldsymbol{Q}}$ included the static pore pressure can be written as:

$$\vec{\boldsymbol{Q}}=\frac{1}{i\omega\rho_w\left(S+if_p\right)}\left[\nabla\left(P+\rho_w g(z-d)\right)-\omega^2\rho_w\vec{\boldsymbol{d}}^*\right] \tag{8}$$

where $\vec{\boldsymbol{d}}^*=\xi\vec{i}+\chi\vec{j}$ is the elastic solid displacement. The derivations of Eqs. (3) and (4) are presented in the Appendix A. Compared to the theory of Lan and Lee (2010), the vertical component of relative velocity in Eq. (8) increases the gradient term of hydrostatic pressure ($\rho_w g$). Eq. (8) can further extend the relevant derivation of the free surface of gravity waves in poroelastic medium. Therefore, the present theory is more suitable for the application of emergent poroelastic medium.

The linear friction factor $f_p$ is the average effect of the total frictional resistance in the poroelastic medium. For the Darcy-Forchheimer flow configuration, $f_p$ can be defined as

$$f_p=\left(\frac{n'\nu}{\omega k_p}\right)+\left(\frac{n'^2 C_f}{\omega\sqrt{k_p}}\right)\left(\frac{\int_\forall\int_t^{t+T}\left|\vec{\boldsymbol{Q}}\right|\vec{\boldsymbol{Q}}\cdot\vec{\boldsymbol{Q}}\;dt\;d\forall}{\int_\forall\int_t^{t+T}\vec{\boldsymbol{Q}}\cdot\vec{\boldsymbol{Q}}\;dt\;d\forall}\right) \tag{9}$$

where $\nu$ is the kinematic viscosity of the fluid, $k_p$ is the intrinsic permeability, $C_f$ is the turbulent drag coefficient, and $\forall$ is the volume of the poroelastic medium. If the fluid frictional resistance in the poroelastic medium satisfies Darcy's law, the linear friction coefficient can be simplified to

$$f_p=\left(\frac{n'\nu}{\omega k_p}\right) \tag{10}$$

## 2. Governing Equations for Water Waves

The fluid domain is divided into regions I and II. The velocity potentials satisfy the Laplace equation given by:

$$\nabla^2\Phi_j=0,\quad j=I,II \tag{11}$$

where $\Phi_I=\Phi^i+\Phi^r$ is the velocity potential in region I and $\Phi^r$ is the reflected velocity potential. The velocity vector related to the potential function is determined by $(\vec{\boldsymbol{q}}_w)_j=\nabla\Phi_j$.

## 3. Boundary Conditions

The bottom boundary and the matching boundary conditions between any adjoining regions must ensure the continuity of the fluid pressure and continuity of normal flow flux. In addition, the normal effective stresses and shear stress on the surfaces of the poro-elastic medium region are equal to zero. As the top of the poro-elastomer exposes the water surface, this study deals with a free surface boundary condition in the context of a poroelastic medium, which has rarely been considered in previous studies. Under linear wave theory, the wave elevation on the free surface boundary $\eta_v$ satisfies:

$$\frac{\partial\eta_v}{\partial t}=Q_z,\quad z=d \tag{12}$$

where $Q_z$ is the vertical component of relative velocity in the

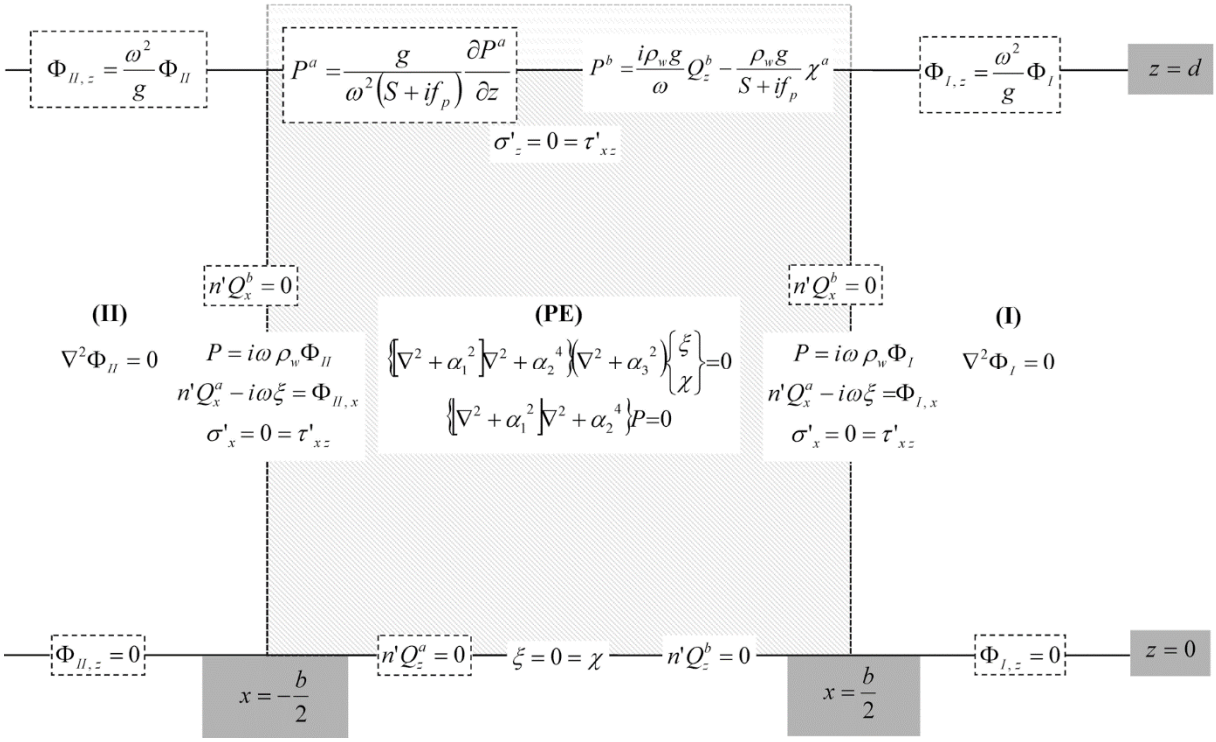


**Fig. 2. Definition of homogeneous boundary value problem considered in this study.**

poroelastic system. As for the dynamic free surface boundary condition in the field of a poroelastic medium, the hydrodynamic pressure $P$ at $z = d$ is equal to the dynamic pressure of the surface elevation ( $\rho_w g\eta_v$ ), i.e.,

$$P=\rho_w g\eta_v, \quad z=d \tag{13}$$

The form of other boundary conditions is similar to that derived by Lan and Lee (2010). The linearized free surface boundary condition can be written as:

$$\frac{\partial\Phi_j}{\partial z}-\frac{\omega^2}{g}\Phi_j=0,\ z=d,\ j=I,II \tag{14}$$

The bottom boundary conditions match the non-slip condition:

$$\frac{\partial\Phi_j}{\partial z}=0,\ z=0,\ j=I,II \tag{15}$$

$$\left.\begin{aligned} n'Q_z&=0\\ \xi&=0\\ \chi&=0\end{aligned}\right\},\ z=0 \tag{16}$$

The boundary conditions on the surface of the poroelastic medium are given by:

$$\sigma'_z=\tau'_{xz}=0,\ z=h_1=d \tag{17}$$

$$\sigma'_x=\tau'_{zx}=0,\ x=\pm\frac{b}{2} \tag{18}$$

where $\sigma'_x$ , $\sigma'_z$ , $\tau'_{xz}$ , and $\tau'_{zx}$ are the effective stresses of the poroelastic medium. The matching boundary conditions between any two adjoining regions ensure the continuity of both the pore pressure and normal flow flux, and are written as:

$$\left.\begin{aligned} P&=i\omega\rho_w\Phi_I\\ n'Q_x-i\omega\xi&=\frac{\partial\Phi_I}{\partial x}\end{aligned}\right\},\ x=\frac{b}{2} \tag{19}$$

$$\left.\begin{aligned} P&=i\omega\rho_w\Phi_{II}\\ n'Q_x-i\omega\xi&=\frac{\partial\Phi_{II}}{\partial x}\end{aligned}\right\},\ x=-\frac{b}{2} \tag{20}$$

## 4. Formulation of the Homogeneous Boundary Value Problem

Based on the linear assumption, the physical properties in region PE are divided into two parts, i.e., $P=P^a+P^b$ , $\xi=\xi^a+\xi^b$ , $\chi=\chi^a+\chi^b$ , $Q_x=Q_x^a+Q_x^b$ , $Q_z=Q_z^a+Q_z^b$ , and so on. Fig. 2 illustrates the separate regions of the boundary value problem, their corresponding governing equations,

and the matching boundary conditions. Using the superscripts *a* and *b*, the boundary value problem can be modified by separating region PE into subregions PE–a and PE–b. Region PE–a satisfies the vertical homogeneous boundary conditions ( $n'Q_z^a = 0,\ z = 0$ and $P^a = g/\left[\omega^2\left(S+if_p\right)\right]\left(\partial P^a/\partial z\right),\ z=d$ ), whereas region PE–b obeys the horizontal homogeneous boundary conditions ( $n'Q_x^b = 0,\ x = \pm b/2$ ). Following this formulation, the homogeneous boundary value problem for waves propagating over a poroelastic medium can be solved analytically.

## III. METHOD OF SOLUTION

The velocity potentials $\Phi^r$ and $\Phi_{II}$ satisfying the Laplace equations, and the free surface and bottom conditions can be obtained formally by the following eigenfunction expansions:

$$\Phi^r = \sum_{n=0}^{\infty} C_{n(I)}\, e^{-\mu_n\left(x-\frac{b}{2}\right)} \cos\mu_n z\, e^{-i\omega t} \tag{21}$$

$$\Phi_{II} = \sum_{n=0}^{\infty} C_{n(II)}\, e^{\mu_n\left(x+\frac{b}{2}\right)} \cos\mu_n z\, e^{-i\omega t} \tag{22}$$

where $\mu_0 = -ik_0$. The eigenvalues $\mu_n$ are determined by the dispersion relation according to $\omega^2 = -g\mu_n \tan\left(\mu_n d\right)$, $n = 0, 1, 2, \ldots$.

Note that both the reflected velocity potential $\Phi^r$ and the transmitted velocity potential $\Phi_{II}$ include propagating ($n = 0$) and evanescent ($n \geq 1$) modes. Thus, the reflection and transmission coefficients can be evaluated by $K_r = \left|C_{0(I)}\right| 2\omega\cosh k_0 d/(gH_i)$ and $K_t = \left|C_{0(II)}\right| 2\omega\cosh k_0 d\,/\,(gH_i)$, respectively. The energy dissipation is estimated using the conservation of wave energy, given by $E_f = 1-(K_r^2 + K_t^2)$. $E_f > 0$ indicates wave damping in the poroelastic medium.

The solution of the system in region PE is obtained by separating the variables. The general solutions of the displacement components and pore pressure, satisfying the homogeneous matching boundary conditions, are given by:

$$\begin{aligned}\xi^a = \sum_{n=0}^{\infty} -\Bigg\{ & \delta_{1n}^a \left( A_{1n}^a\, e^{\delta_{1n}^a\left(x-\frac{b}{2}\right)} - A_{2n}^a\, e^{-\delta_{1n}^a\left(x+\frac{b}{2}\right)} \right) \\ & + \delta_{2n}^a \left( A_{3n}^a\, e^{\delta_{2n}^a\left(x-\frac{b}{2}\right)} - A_{4n}^a\, e^{-\delta_{2n}^a\left(x+\frac{b}{2}\right)} \right) \\ & + \left(\frac{\hat{\mu}_n^{a2}}{\delta_{3n}^a}\right) \left( A_{5n}^a\, e^{\delta_{3n}^a\left(x-\frac{b}{2}\right)} - A_{6n}^a\, e^{-\delta_{3n}^a\left(x+\frac{b}{2}\right)} \right) \Bigg\} \cos\left(\hat{\mu}_n^a z\right) e^{-i\omega t}\end{aligned} \tag{23}$$

$$\begin{aligned}\chi^a = \sum_{n=0}^{\infty} \hat{\mu}_n^a \Bigg\{ & \left( A_{1n}^a e^{\delta_{1n}^a\left(x-\frac{b}{2}\right)} + A_{2n}^a e^{-\delta_{1n}^a\left(x+\frac{b}{2}\right)} \right) \\ & + \left( A_{3n}^a e^{\delta_{2n}^a\left(x-\frac{b}{2}\right)} + A_{4n}^a e^{-\delta_{2n}^a\left(x+\frac{b}{2}\right)} \right) \\ & + \left( A_{5n}^a e^{\delta_{3n}^a\left(x-\frac{b}{2}\right)} + A_{6n}^a e^{-\delta_{3n}^a\left(x+\frac{b}{2}\right)} \right) \Bigg\} \sin\left(\hat{\mu}_n^a z\right) e^{-i\omega t}\end{aligned} \tag{24}$$

$$\begin{aligned}P^a = \sum_{n=0}^{\infty} \omega^2 \rho_w \left( \frac{S+if_p}{n'} - 1 \right) \Bigg\{ & \Lambda_{1n}^a \left( A_{1n}^a e^{\delta_{1n}^a\left(x-\frac{b}{2}\right)} + A_{2n}^a e^{-\delta_{1n}^a\left(x+\frac{b}{2}\right)} \right) \\ & + \Lambda_{2n}^a \left( A_{3n}^a e^{\delta_{2n}^a\left(x-\frac{b}{2}\right)} + A_{4n}^a e^{-\delta_{2n}^a\left(x+\frac{b}{2}\right)} \right) \Bigg\} \cos\left(\hat{\mu}_n^a z\right) e^{-i\omega t}\end{aligned} \tag{25}$$

where the eigenvalues $\hat{\mu}_n^a$ are determined by the dispersion relation as:

$$\omega^2\left(S+if_p\right) = -g\hat{\mu}_n^a \tan\left(\hat{\mu}_n^a d\right),\ n = 0, 1, 2, \ldots \tag{26}$$

Similarly,

$$\begin{aligned}\xi^b = \sum_{n=0}^{\infty} \hat{\mu}_n^b \Bigg\{ & \left( A_{1n}^b e^{\delta_{1n}^b(z-d)} + A_{2n}^b e^{-\delta_{1n}^b(z-d)} \right) \\ & + \left( A_{3n}^b e^{\delta_{2n}^b(z-d)} + A_{4n}^b e^{-\delta_{2n}^b(z-d)} \right) \\ & + \left( A_{5n}^b e^{\delta_{3n}^b(z-d)} + A_{6n}^b e^{-\delta_{3n}^b(z-d)} \right) \Bigg\} \sin\hat{\mu}_n^b \left( x-\frac{b}{2} \right) e^{-i\omega t}\end{aligned} \tag{27}$$

$$\begin{aligned}\chi^b = \sum_{n=0}^{\infty} -\Bigg\{ & \delta_{1n}^b \left( A_{1n}^b e^{\delta_{1n}^b(z-d)} - A_{2n}^b e^{-\delta_{1n}^b(z-d)} \right) \\ & + \delta_{2n}^b \left( A_{3n}^b e^{\delta_{2n}^b(z-d)} - A_{4n}^b e^{-\delta_{2n}^b(z-d)} \right) \\ & + \left( \frac{\hat{\mu}_n^{b2}}{\delta_{3n}^b} \right) \left( A_{1n}^b e^{\delta_{1n}^b(z-d)} - A_{2n}^b e^{-\delta_{1n}^b(z-d)} \right) \Bigg\} \cos\hat{\mu}_n^b \left( x-\frac{b}{2} \right) e^{-i\omega t}\end{aligned} \tag{28}$$

$$\begin{aligned}P^b = \sum_{n=0}^{\infty} \omega^2 \rho_w \left( \frac{S+if_p}{n'} - 1 \right) \Bigg\{ & \Lambda_{1n}^b \left( A_{1n}^b e^{\delta_{1n}^b(z-d)} + A_{2n}^b e^{-\delta_{1n}^b(z-d)} \right) \\ & + \Lambda_{2n}^b \left( A_{3n}^b e^{\delta_{2n}^b(z-d)} + A_{4n}^b e^{-\delta_{2n}^b(z-d)} \right) \Bigg\} \cos\hat{\mu}_n^b \left( x-\frac{b}{2} \right) e^{-i\omega t}\end{aligned} \tag{29}$$

where

$$\hat{\mu}_n^b = n\pi/b\,, \quad n = 0, 1, 2, \ldots \tag{30}$$

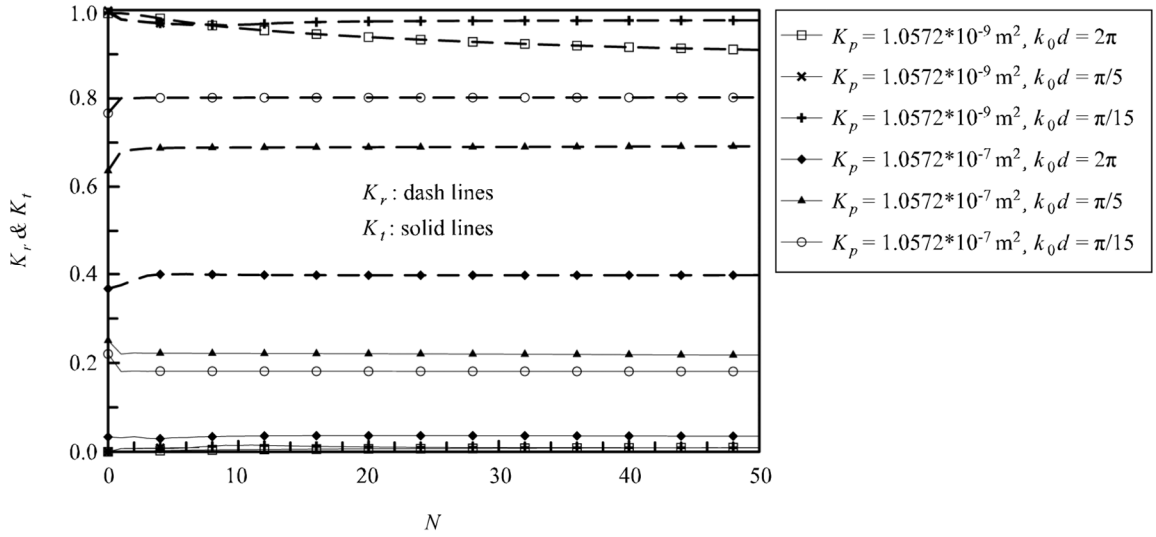


**Fig. 3. Reflection and transmission coefficients versus the number of adopted wave modes.**

$$(\delta_{\ell n}^{\psi})^2 = \left[ (\hat{\mu}_n^{\psi})^2 - \frac{(\alpha_1)^2}{2} \right] + (-1)^{\ell} \sqrt{\frac{(\alpha_1)^4}{4} - (\alpha_2)^4} \ , \psi = a,b \ , \quad \ell = 1, 2 \tag{31}$$

$$(\delta_{3n}^{\psi})^2 = (\hat{\mu}_n^{\psi})^2 - (\alpha_3)^2 \ , \quad \psi = a,b \tag{32}$$

$$\Lambda_{\ell n}^{\psi} = \frac{(\hat{\mu}_n^{\psi})^2 - (\delta_{\ell n}^{\psi})^2}{(\hat{\mu}_n^{\psi})^2 - (\delta_{\ell n}^{\psi})^2 - \omega^2 \rho_w \beta (S + i f_p)} \ , \psi = a,b \ , \quad \ell = 1, 2 \tag{33}$$

The 14 quantities $C_{n(I)}$, $C_{n(II)}$, $A_{1n}^{a} - A_{6n}^{a}$, and $A_{1n}^{b} - A_{6n}^{b}$ are unknowns that must be determined by power series approximations. Note that Eqs (13), (16)-(20) form a linear system of 14 equations. These unknowns can be obtained using the remaining matching boundary conditions together with the orthogonal eigenvalues $\mu_n$, $\hat{\mu}_n^{a}$, and $\hat{\mu}_n^{b}$. The detailed matrix equations are presented in the Appendix B.

## IV. VERIFICATION

The present wave theory includes evanescent wave series for which the number of modes used in the computation must be determined. Fig. 3 demonstrates the computed reflection and transmission coefficients with respect to the number of modes used in the theory. The conditions used in the computations are $k_0d = 2\pi$, $\pi/5$, $\pi/15$, $H_i/d = 0.01$, $b/d = 1$, $h/d = 1.0285$, $n' = 0.439$, $C_f = 0.295$, $S = 1.015$, $\mu = 0.333$, $\rho_s = 2650$ kg/m$^3$, $\rho_w = 1000$ kg/m$^3$, $\nu = 1.12\times10^{-6}$ m$^2$/s, $\beta = 4.35\times10^{-10}$ m$^2$/N, $G = 1\times10^5$ N/m$^2$, with $k_p = 1.0572\times10^{-9}$ m$^2$ to simulate low permeability and $k_p = 1.0572\times10^{-7}$ m$^2$ to model higher permeability. The calculation conditions cover deep water waves ($k_0d = 2\pi$), intermediate water waves ($k_0d = \pi/5$), and shallow water waves ($k_0d = \pi/15$), as well as different permeabilities ($k_p$). The results show that, with approximately 30 modes, the wave reflection and transmission coefficients converge in all six cases.

The present theory is being used to approximate the problem of waves passing over an impermeable and rigid structure. Small values of the porosity ($n' = 1\times10^{-7}$), intrinsic permeability ($k_p = 0$, i.e., $f_p = 0$), turbulent drag coefficient ($C_f = 0$), unit virtual mass coefficient ($S = 1$), and rigid-type shear modulus ($G = 1.125\times10^{10}$ N/m$^2$) are used in the calculations. Fig. 4 shows the reflection coefficient $K_r$ and transmission coefficient $K_t$ with respect to $k_0d$, where $b/d = 1$ and $h/d = 1.0285$. The comparisons show that the present theory matches the analytic solutions ($K_r = 1$ and $K_t = 0$) very well.

For the case of a porous and rigid breakwater, the experimental results reported by Sollitt and Cross (1972) are used for comparison. In their experiments, the water depth $d$ = 0.3048 m, the incident wave height remains within $0.008 < H_i/L_0 < 0.012$ ($L_0$ is the incident wave length), nd the coefficient $k_0d = 0.5 - 2.5$. For a permeable breakwater, the porosity $n' = 0.439$, the intrinsic permeability $k_p = 1.0572\times10^{-7}$ m$^2$, and the turbulent drag coefficient $C_f = 0.295$. The other conditions used in the computations are $b/d = 1$, $h/d = 1.0285$, $S = 1.015$, $\mu = 0.333$, $\rho_s = 2650$ kg/m$^3$, $\rho_w = 1000$ kg/m$^3$, $\nu = 1.12\times10^{-6}$ m$^2$/s, $\beta = 4.35\times10^{-10}$ m$^2$/N, and $G = 1.125\times10^{10}$ N/m$^2$. The experimental model of Sollitt and Cross (1972) has high permeability with turbulent resistance, so Darcy-Forchheimer flow configuration is used to this calculation. The wave reflection and transmission coefficients with respect to $k_0d$ are compared in Fig. 5. The results of Sollitt and Cross (1972) are also plotted. This comparison shows that the present theory is in good agreement with experimental data.

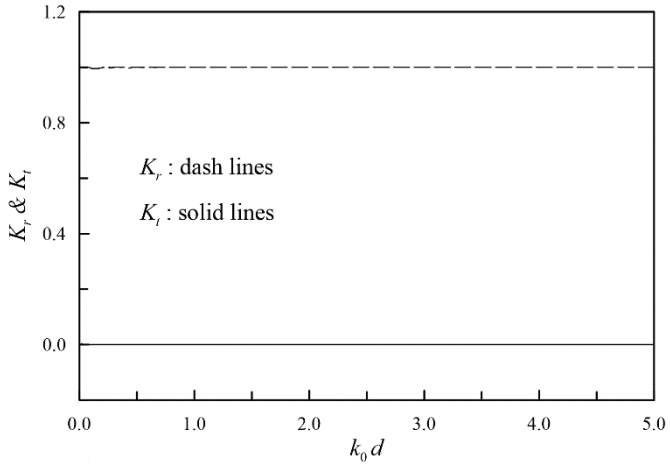


**Fig. 4. Reflection coefficient $K_r$ and transmission coefficient $K_t$ versus $k_0d$ for a rigid and impermeable breakwater ($b/d$ = 1, $h/d$ = 1.0285).**

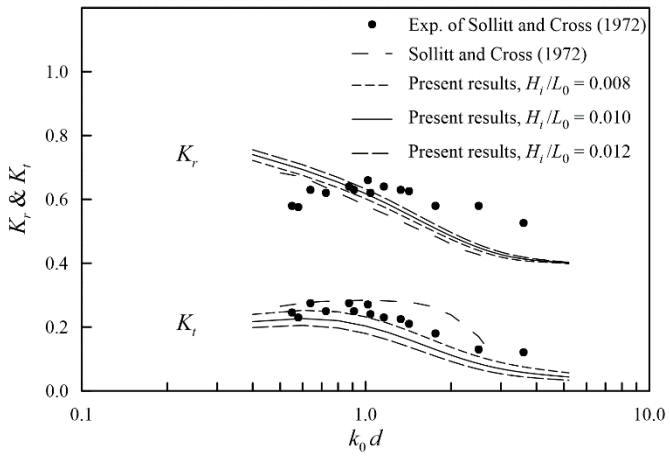


**Fig. 5. Comparison of the present theory with the solution and experimental data of Sollitt and Cross (1972) for the case of a wave passing over a single permeable breakwater.**

## V. COMPUTATIONAL RESULTS

In this section, the effects of the flexibility and permeability of the poroelastic medium on wave transformation (e.g., wave reflection, transmission, and energy dissipation) are studied in detail. The physical conditions of the poroelastic media and water waves used for the computations are listed in Table 1, where Case A examines the effect of elasticity and Case B studies permeability. The frictional resistance in porous elastic media is taken into account the type of Darcy-Forchheimer flow configuration.

The key parameters in Table 1 ($G$, $n'$ and $k_p$) basically are chosen according to the experiment study of Lan (2000) and Lan et al. (2011) for soft materials, and Sollitt and Cross (1972) for rigid structures. For model applications, the soft materials of the sea-grass vegetation, sponges and polymer foams can be used in the practical design. The change of the

**Table 1. Physical properties of poroelastic media and water waves.**

| Properties | Case A | Case B |
|---|---|---|
| $b/d$ | 1.0 | 1.0 |
| | 0.5 | 0.5 |
| $h/d$ | 1.0285 | 1.0285 |
| $n'$ | 0.439 | 0.439 |
| $\mu$ | 0.333 | 0.333 |
| $H_i$/L0 | 0.01 | 0.01 |
| $G$(N/m$^2$) | $1 \times 10^8$ | $1 \times 10^8$ |
| | $1 \times 10^6$ | |
| | $1 \times 10^5$ | $1 \times 10^4$ |
| | $5 \times 10^4$ | |
| | $1 \times 10^4$ | |
| $\nu$ (m$^2$/s) | $1.12 \times 10^{-6}$ | $1.12 \times 10^{-6}$ |
| $\beta$(m$^2$/N) | $4.35 \times 10^{-10}$ | $4.35 \times 10^{-10}$ |
| $C_f$ | 0.295 | 0.295 |
| $S$ | 1.015 | 1.015 |
| $\rho_s$ (kg/m$^3$) | 2650 | 2650 |
| $\rho_w$ (kg/m$^3$) | 1000 | 1000 |
| $k_p$(m$^2$) | $5.2860 \times 10^{-9}$ | $1.0572 \times 10^{-7}$ |
| | | $1.0572 \times 10^{-8}$ |
| | | $5.2860 \times 10^{-9}$ |

shear modulus $G$ represents the soft or hard and rigid material, for example, $G = 10^4 - 10^5$ N/m$^2$ is for the case of sponges and polymer foams (Lan, 2000; Lan et al., 2011), $G = 10^5 - 10^6$ N/m$^2$ is for the case of rubbers and $G \geq 10^8$ N/m$^2$ is for hard and rigid materials (Gere and Timoshenko, 1984). In addition, the permeability coefficient $k_p$ is generally between $10^{-7}$ m$^2$ (high permeability) and $10^{-9}$ m$^2$ (low permeability) when the porosity $n'$ is around 0.4 (Sollitt and Cross, 1972; Hsu et al., 1993). To examine the effect of shear modulus and permeability, numerical parameters are set to have the same values for comparison.

### 1. Effect of Shear Modulus of the Poroelastic Medium

Figs. 6 and 7 show the reflection coefficient $K_r$, transmission coefficient $K_t$, and wave energy dissipation $E_f$ versus $k_0d$ for five materials with shear moduli of $G = 1 \times 10^8$, $1 \times 10^6$, $1 \times 10^5$, $5 \times 10^4$, $1 \times 10^4$ N/m$^2$ and material permeability $k_p = 5.286 \times 10^{-9}$ m$^2$. The dimensionless width $b/d$ is 1.0 and 0.5 in Figs. 6 and 7, respectively. The results of Fig. 6 show that when $G$ is greater than $10^6$ N/m$^2$, the effect of material elasticity on the waves is negligible. The wave reflection and transmission approach that of a rigid permeable structure constricted from stiff materials. For smaller value of the shear modulus ($G < 10^6$ N/m$^2$), the effect of elasticity on wave transformation is obvious. As $G$ decreases, the reflection coefficient $K_r$ decreases and the transmission coefficient $K_t$ increase. These results are caused by the motions of the elastic solid and pore fluid, with frictional resistance induced to dissipate the internal energy. The reflection coefficient, transmission

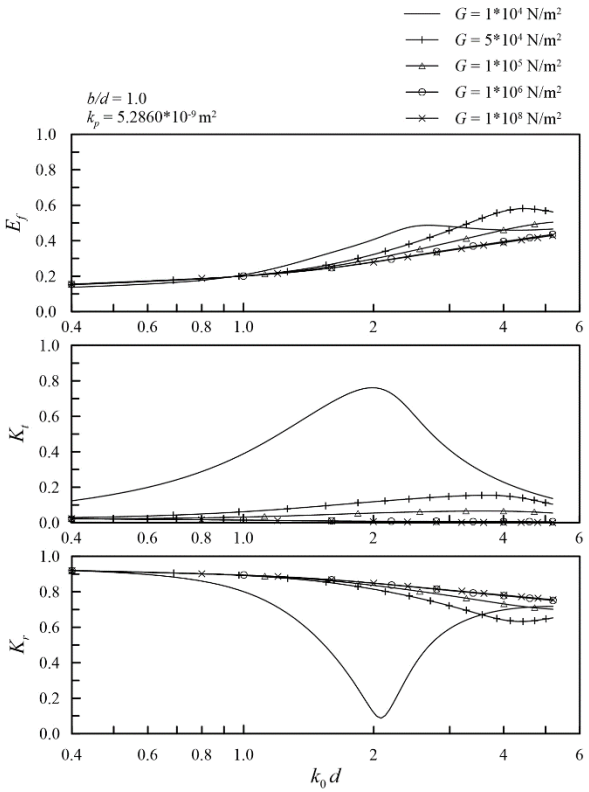


**Fig. 6. $K_r$, $K_t$, and $E_f$ versus $k_0d$ for varying shear modulus $G$ ($b/d$ = 1.0, $k_p = 5.286 \times 10^{-9}$ m$^2$, Darcy-Forchheimer flow configuration).**

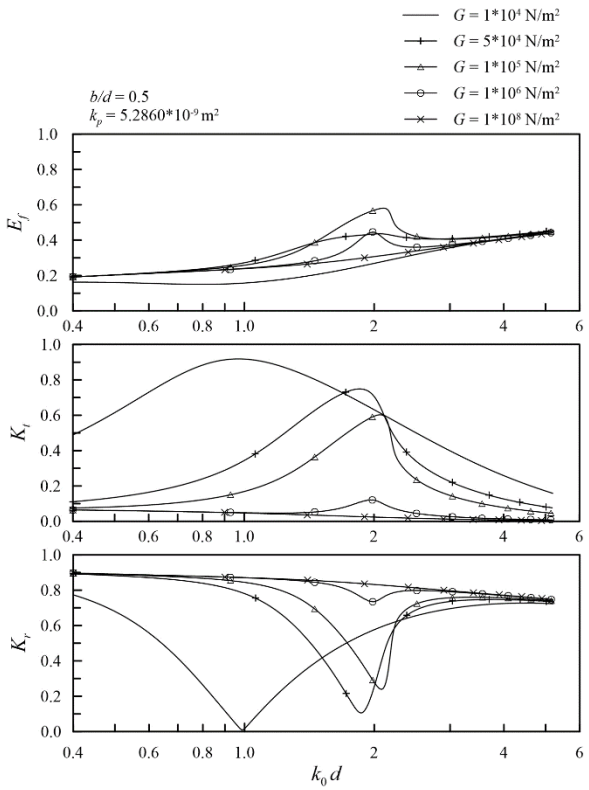


**Fig. 7. $K_r$, $K_t$, and $E_f$ versus $k_0d$ for varying shear modulus $G$ ($b/d$ = 0.5, $k_p = 5.286 \times 10^{-9}$ m$^2$, Darcy-Forchheimer flow configuration).**

coefficient and wave energy variation with $k_0d$ are related to the phase lag between wave motion and medium deformation (Lan and Lee, 2010). Fig. 7 illustrates that the smaller medium width, the greater the flexural deformation induced by wave force, and the more obvious change in wave reflection, transmission and energy dissipation. As $G$ is smaller, the extreme values of $K_r$ and $K_t$ are basically shifted to smaller $k_0d$.

## 2. Effect of Permeability of the Poroelastic Medium

The effects of the permeability of the emergent poroelastic medium on wave reflection $K_r$, transmission $K_t$, and energy dissipation $E_f$ are studied in the section. Figs. 8 and 9 show $K_r$, $K_t$, and $E_f$ versus $k_0d$ for $k_p = 5.286 \times 10^{-9} - 1.0572 \times 10^{-7}$ m$^2$. For stiff media ($G = 1 \times 10^8$ N/m$^2$), the effects of permeability on waves are similar to the case of rigid and porous media (Lan and Lee, 2010). The results show that the wave reflection $K_r$ and transmission $K_t$ decrease with increasing $k_0d$, and the energy dissipation $E_f$ increases with the increase of $k_0d$. With an increase in medium permeability $k_p$, the wave reflection coefficient $K_r$ diminishes and the wave transmission $K_t$ increases. Higher permeability induces higher frictional resistance inside the stiff poroelastic medium, which induces higher energy dissipation.

For soft structures ($G = 1 \times 10^4$ N/m$^2$), Figs. 10 and 11 show that resonance occurs respectively at $k_0d \approx 1.81$ and 1.03 for the impermeable case. The phenomenon of quasi-resonance appears in the interval $1.0 < k_0d < 4.0$ for permeable cases. The phase lag of the medium vibration and wave oscillation is the cause of the minimum $K_r$ and maximum $K_t$ at a particular value of $k_0d$. The extreme values of reflection and transmission coefficients shift to the large $k_0d$ value as the intrinsic permeability $k_p$ increases. This quasi-resonance is caused by the composite effects of medium deformation and frictional damping induced by the seepage velocity of the interactive mechanism between waves and the poroelastic medium.

## 3. Effect of Frictional Resistance Type of the Poroelastic Medium

Figs. 12 and 13 show the wave reflection $K_r$, transmission $K_t$, and energy dissipation $E_f$ versus $k_0d$ for the intrinsic permeability $k_p$ from $5.286 \times 10^{-9}$ to $1.0572 \times 10^{-7}$ m$^2$ with Darcy friction resistance. It is well known that the porous friction properties of various materials affect the variatins of wave scattering and dissipation. Comparisons of Figs. 8 and 12 and Figs. 10 and 13 illustrate different types of frictional resistance in poroelastic media have obvious variability to the effects of wave reflection, transmission and wave damping. This means that in practical applications, the friction characteristics of permeable material need to be calibrated in advance to determine which friction resistance flow configuration.

# VI. CONCLUSION

This paper has presented an analytical solution for waves

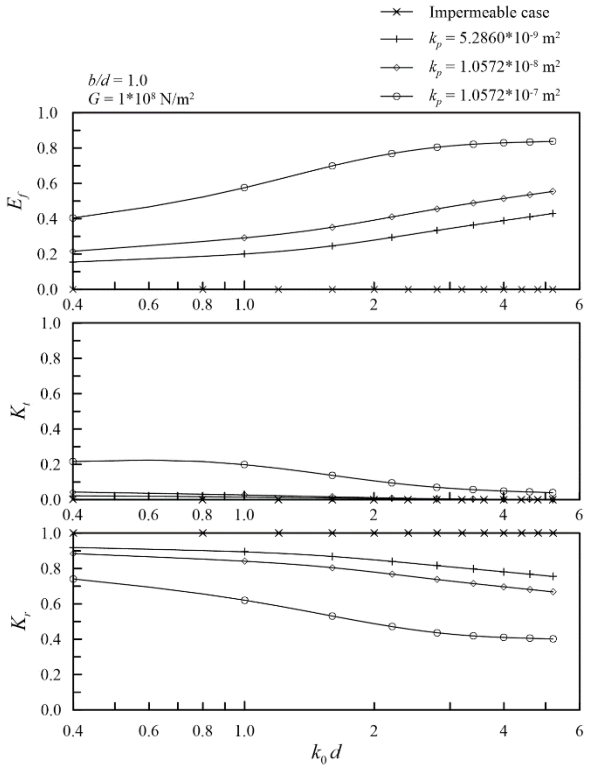


**Fig. 8.** $K_r$, $K_t$, and $E_f$ versus $k_0 d$ for varying intrinsic permeability $k_p$ ($b/d$ = 1.0, $G = 1 \times 10^8$ N/m$^2$, Darcy-Forchheimer flow configuration).

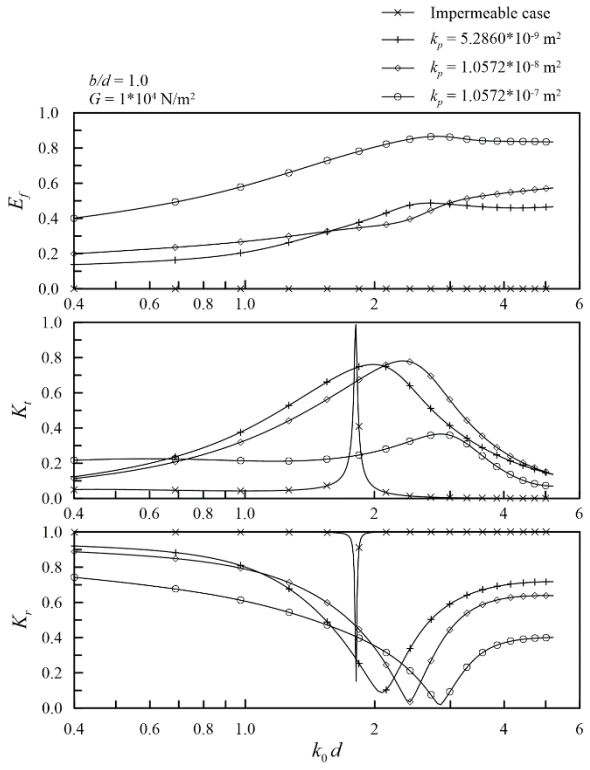


**Fig. 10.** $K_r$, $K_t$, and $E_f$ versus $k_0 d$ for varying intrinsic permeability $k_p$ ($b/d$ = 1.0, $G = 1 \times 10^4$ N/m$^2$, Darcy-Forchheimer flow configuration).

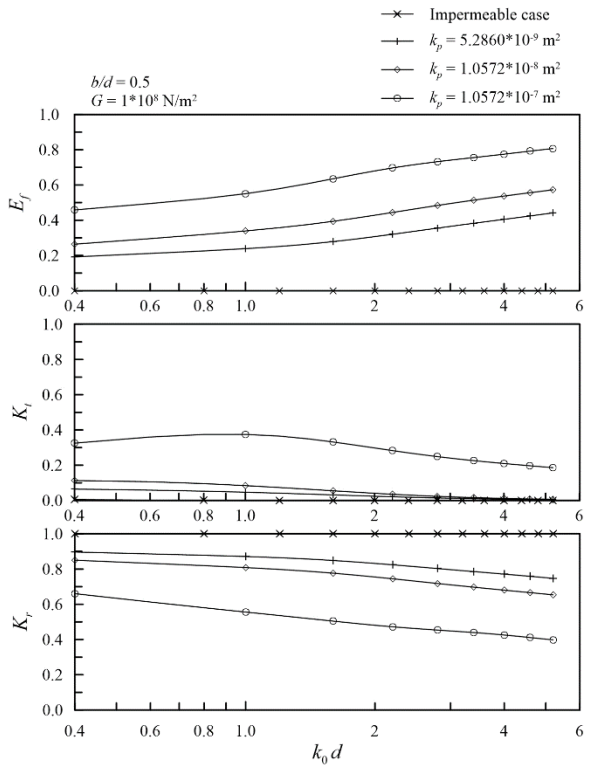


**Fig. 9.** $K_r$, $K_t$, and $E_f$ versus $k_0 d$ for varying intrinsic permeability $k_p$ ($b/d$ = 0.5, $G = 1 \times 10^8$ N/m$^2$, Darcy-Forchheimer flow configuration).

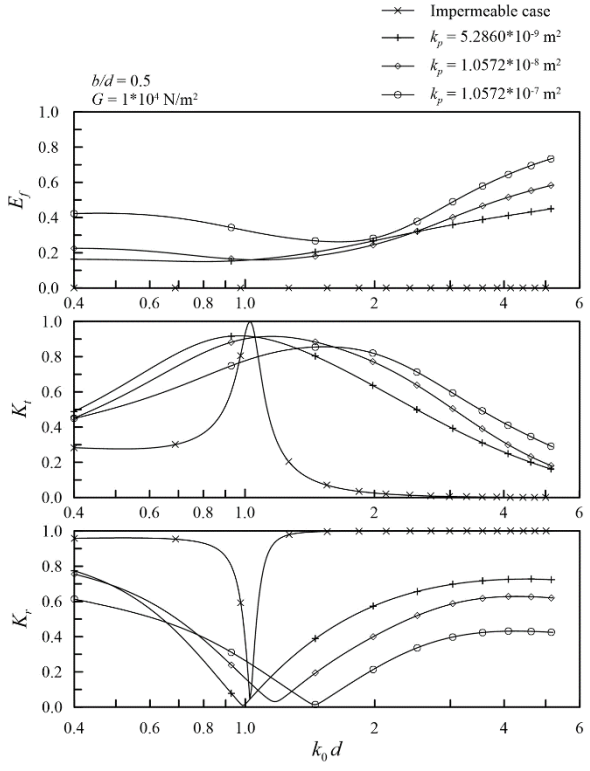


**Fig. 11.** $K_r$, $K_t$, and $E_f$ versus $k_0 d$ for varying intrinsic permeability $k_p$ ($b/d$ = 0.5, $G = 1 \times 10^4$ N/m$^2$, Darcy-Forchheimer flow configuration).

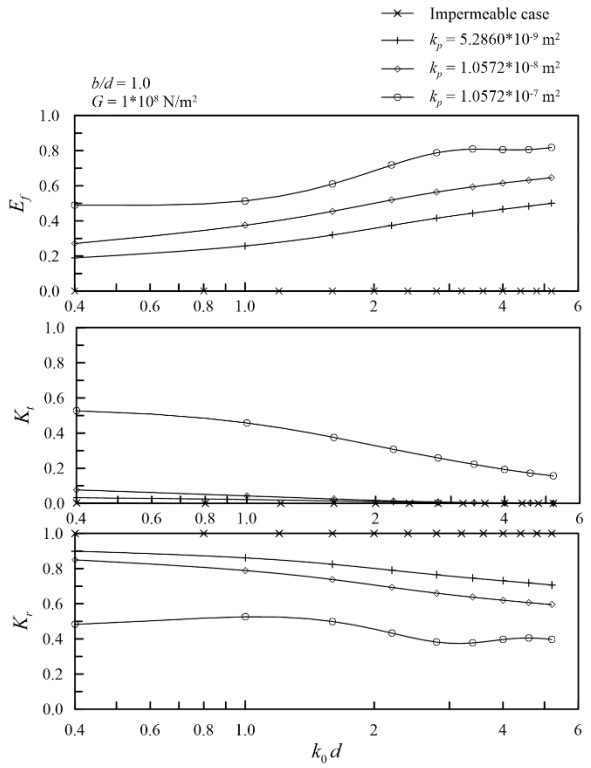


**Fig. 12.** $K_r$, $K_t$, and $E_f$ versus $k_0 d$ for varying intrinsic permeability $k_p$ ($b/d = 1.0$, $G = 1 \times 10^8$ N/m$^2$, Darcy flow configuration).

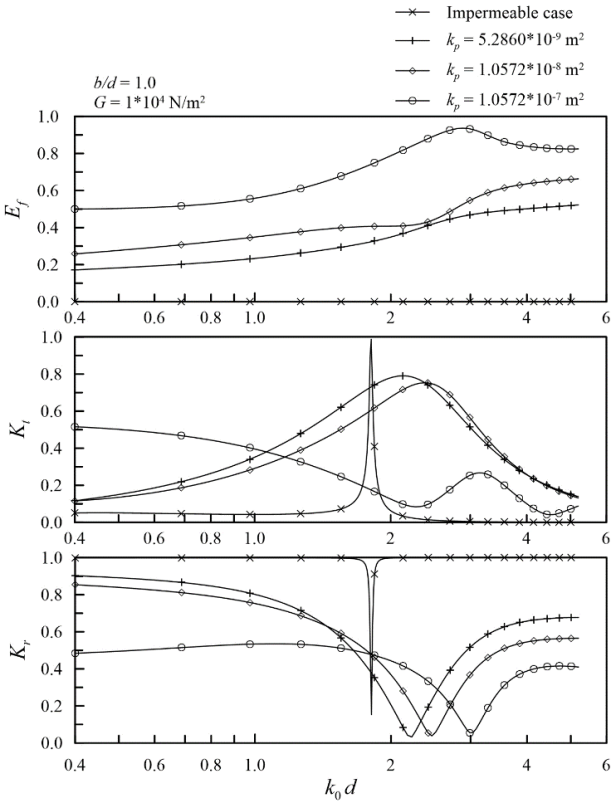


**Fig. 13.** $K_r$, $K_t$, and $E_f$ versus $k_0 d$ for varying intrinsic permeability $k_p$ ($b/d = 1.0$, $G = 1 \times 10^4$ N/m$^2$, Darcy flow configuration).

propagating over an emergent poroelastic medium. An improved poroelastic theory has been developed based on Lan-Lee's poro-elastomer theory and consideration of the static pore pressure. The interactions between waves and the poroelastic medium were considered through the continuity of the flow flux and pressure on the interfacial boundaries. Free surface boundary conditions in the field of poroelastic media were also proposed. Numerical results compare well with simplified cases of impermeable and rigid structures, as well as experimental results for porous structures (Sollitt and Cross, 1972). On the basis of the results from this study, the following major conclusions can be drawn.

1. The shear modulus of the emergent poroelastic medium is a key factor affecting wave transformation in the region $G < 10^6 \,\mathrm{N/m^2}$.
2. Resonance phenomena induced by structural vibration and wave oscillation can occur on softer and almost impermeable structures. Higher permeability induces significant wave damping and reduces the resonance through interaction between the waves and the poroelastic medium.
3. Different frictional resistance models of poroelastic medium have high variability of effect on the wave scattering.

The present conclusions provide considerations for the design of wave-prevention structures for different materials. We can change the permeability of rigid structures to increase the attenuation of wave energy and reduce wave reflection and transmission, thus achieving superior wave-defense effects. When using flexible materials, we need to prevent quasi-resonance from occurring in the period range of frequent waves at the defensive site; if this is unavoidable, the flexible structure could be designed to have a poro-flexible configuration with permeable properties to suppress resonance. The present theory and solution provide a theoretical and general way to investigate wave transformation problems over any material structures.

The experimental verification results of the submerged poroelastic medium have proved the rationality of Lan-Lee's poro-elastomer theory (Lan, 2000; Lan et al., 2011). However, there are relatively few studies on the numerical results and experimental data to the verification of the present analytic solution for this paper. It is necessary to focus on the issue by more researches of relevant experiments, field observations and numerical simulations. The mutual verification between the subsequent researches and the analytical solution of this paper could expand the breadth of investigation on this topic. For the subsequent research of the interaction between waves and floating poroelastic media, the freedom of motion of the floating bodies and the water surface variation in the floating media increase the complexity of the analysis. The free surface boundary condition of emergent poroelastic media proposed in this paper can provide a solution to deal with the free surface boundary. Future researches will investigate applications to actual analysis of waves passing over emergent

vegetation and the development of wave absorbers for ocean engineering and marine biology. In addition, nonlinear effect of waves is one of an important research topics for the interaction between waves and poroelastic media.

## ACKNOWLEDGMENTS

This research was financially supported by the Ministry of Science and Technology, Taiwan, under grant no. MOST 106-2221-E-019-034.

## APPENDIX A

Extended Lan-Lee's poro-elastomer theory (Lan and Lee, 2010) for consideration of static pore pressure ( $\rho_w g(z-d)$ ), the conservation of mass and the conservation of momentum for the wave field are satisfied:

$$\frac{\partial P}{\partial t} = -\frac{1}{n'\beta}\left[\nabla\cdot\left(\frac{\partial \vec{\boldsymbol{d}}^*}{\partial t}\right)+n'\nabla\cdot\vec{\boldsymbol{Q}}\right] \tag{34}$$

and

$$\nabla\cdot\boldsymbol{\tau}^* -(1-n')\nabla\left(P+\rho_w g(z-d)\right) = (1-n')\rho_s\frac{\partial^2 \vec{\boldsymbol{d}}^*}{\partial t^2}-n'\rho_w\left(S-1\right)\frac{\partial \vec{\boldsymbol{Q}}}{\partial t}-n'\rho_w\left(\frac{n'\nu}{k_p}\right)\vec{\boldsymbol{Q}} \quad -n'\rho_w\left(\frac{n'^2 C_f}{\sqrt{k_p}}\right)\left|\vec{\boldsymbol{Q}}\right|\vec{\boldsymbol{Q}} \tag{35}$$

$$-n'\nabla\left(P+\rho_w g(z-d)\right) = n'\rho_w\frac{\partial^2 \vec{\boldsymbol{d}}^*}{\partial t^2}+n'\rho_w S\frac{\partial \vec{\boldsymbol{Q}}}{\partial t}+n'\rho_w\left(\frac{n'\nu}{k_p}\right)\vec{\boldsymbol{Q}} \quad +n'\rho_w\left(\frac{n'^2 C_f}{\sqrt{k_p}}\right)\left|\vec{\boldsymbol{Q}}\right|\vec{\boldsymbol{Q}} \tag{36}$$

where $\nabla=(\partial/\partial x,\partial/\partial z)$ is the gradient operator, $\vec{\boldsymbol{Q}}$ is the fluid velocity relative to the elastic solid, and $\tau^*$ is the effective stress tensor of poroelastic media.

The right-hand sides of Eqs. (35) and (36) include two force components. The first and second terms represent the inertia force, whereas the third and last terms represent the Darcy-Forchheimer resistance force. The Darcy-Forchheimer flow configuration and Lorentz's hypothesis have been applied to deal with the turbulent resistance force and linearize the governing equations, respectively (Lan and Lee, 2010). The linear friction factor $f_p$, which is the average effect of the total frictional resistance in the poroelastic medium, can be defined as

$$\int_\forall\int_t^{t+T}\left(\omega f_p\,\vec{\boldsymbol{Q}}\right)\cdot\vec{\boldsymbol{Q}}\,dt\;\;d\forall=\int_\forall\int_t^{t+T}\left(\frac{n'\nu}{k_p}\vec{\boldsymbol{Q}}+\frac{n'^2 C_f}{\sqrt{k_p}}\left|\vec{\boldsymbol{Q}}\right|\vec{\boldsymbol{Q}}\right)\cdot\vec{\boldsymbol{Q}}\;\;dt\;\;d\forall \tag{37}$$

Substituting the linearized relationship into Eqs. (35) and (36), the coupled momentum equations for the poroelastic medium can be simplified as:

$$\nabla\cdot\boldsymbol{\tau}^* -(1-n')\nabla\left(P+\rho_w g(z-d)\right) = (1-n')\rho_s\frac{\partial^2 \vec{\boldsymbol{d}}^*}{\partial t^2}-n'\rho_w\left(S-1\right)\frac{\partial \vec{\boldsymbol{Q}}}{\partial t}-n'\omega\rho_w f_p\,\vec{\boldsymbol{Q}} \tag{38}$$

$$-n'\nabla\left(P+\rho_w g(z-d)\right) = n'\rho_w\frac{\partial^2 \vec{\boldsymbol{d}}^*}{\partial t^2}+n'\rho_w S\frac{\partial \vec{\boldsymbol{Q}}}{\partial t}+n'\omega\rho_w f_p\,\vec{\boldsymbol{Q}} \tag{39}$$

The relationship between the effective stresses and strains in the poroelastic medium is governed by Hooke's law:

$$\boldsymbol{\tau}^* = \begin{Bmatrix}\sigma'_x & \tau'_{zx}\\ \tau'_{xz} & \sigma'_z\end{Bmatrix} = \begin{Bmatrix} 2G\left(\frac{\partial\xi}{\partial x}+\frac{\mu}{1-2\mu}(\nabla\cdot\vec{\boldsymbol{d}}^*)\right) & G\left(\frac{\partial\chi}{\partial x}+\frac{\partial\xi}{\partial z}\right)\\ G\left(\frac{\partial\chi}{\partial x}+\frac{\partial\xi}{\partial z}\right) & 2G\left(\frac{\partial\chi}{\partial z}+\frac{\mu}{1-2\mu}(\nabla\cdot\vec{\boldsymbol{d}}^*)\right)\end{Bmatrix} \tag{40}$$

Eqs. (34), (38), (39), and (40) can be decoupled into three partial differential equations (PDEs) in $\xi$, $\chi$, and $P$ as Eqs. (3) and (4). In addition, note that Eq. (39) is used to obtain $\vec{Q}$ after$\xi$, $\chi$, and $P$ have been determined as Eq. (15).

## APPENDIX B

Substituting the solutions expressed by Eqs (21)-(25) and (27)-(29) into the corresponding matching boundary conditions in Eqs. (13) and (16)-(20), and applying their orthogonality, the following equations are obtained:

$$\begin{aligned}
&\frac{b}{2}\left(1+\delta_{0m}\right)\left\{\left[\omega^2\rho_w\left(\frac{S+if_p}{n'}-1\right)\Lambda_{1m}^b-\frac{\rho_w g\delta_{1m}^b}{S+if_p}\left(\left(\frac{S+if_p}{n'}-1\right)\Lambda_{1m}^b+1\right)\right]A_{1m}^b\right.\\
&+\left[\omega^2\rho_w\left(\frac{S+if_p}{n'}-1\right)\Lambda_{1m}^b+\frac{\rho_w g\delta_{1m}^b}{S+if_p}\left(\left(\frac{S+if_p}{n'}-1\right)\Lambda_{1m}^b+1\right)\right]A_{2m}^b\\
&+\left[\omega^2\rho_w\left(\frac{S+if_p}{n'}-1\right)\Lambda_{2m}^b-\frac{\rho_w g\delta_{2m}^b}{S+if_p}\left(\left(\frac{S+if_p}{n'}-1\right)\Lambda_{2m}^b+1\right)\right]A_{3m}^b\\
&+\left[\omega^2\rho_w\left(\frac{S+if_p}{n'}-1\right)\Lambda_{2m}^b+\frac{\rho_w g\delta_{2m}^b}{S+if_p}\left(\left(\frac{S+if_p}{n'}-1\right)\Lambda_{2m}^b+1\right)\right]A_{4m}^b\\
&\left.-\frac{\rho_w g}{S+if_p}\frac{\hat{\mu}_m^{b2}}{\delta_{3m}^b}\left(A_{5m}^b-A_{6m}^b\right)\right\}+\sum_{n=0}^{\infty}\frac{\rho_w g}{S+if_p}\hat{\mu}_n^a\sin\hat{\mu}_n^a d\left\{\delta_{1n}^a\left(\mathrm{E}_{1nm}^{ab}A_{1n}^a+\mathrm{F}_{1nm}^{ab}A_{2n}^a\right)\right.\\
&\left.+\delta_{2n}^a\left(\mathrm{E}_{2nm}^{ab}A_{3n}^a+\mathrm{F}_{2nm}^{ab}A_{4n}^a\right)+\delta_{3n}^a\left(\mathrm{E}_{3nm}^{ab}A_{5n}^a+\mathrm{F}_{3nm}^{ab}A_{6n}^a\right)\right\}=0,\qquad m=0,1,2,\ldots
\end{aligned}\tag{41}$$

$$\delta_{1m}^b\Lambda_{1m}^b\left(e^{-\delta_{1m}^b d}A_{1m}^b-e^{\delta_{1m}^b d}A_{2m}^b\right)+\delta_{2m}^b\Lambda_{2m}^b\left(e^{-\delta_{2m}^b d}A_{3m}^b-e^{\delta_{2m}^b d}A_{4m}^b\right)=0,\qquad m=0,1,2,\ldots\tag{42}$$

$$\begin{aligned}
&\frac{b}{2}\hat{\mu}_m^b\left\{\left(e^{-\delta_{1m}^b d}A_{1m}^b+e^{\delta_{1m}^b d}A_{2m}^b\right)+\left(e^{-\delta_{2m}^b d}A_{3m}^b+e^{\delta_{2m}^b d}A_{4m}^b\right)+\left(e^{-\delta_{3m}^b d}A_{5m}^b+e^{\delta_{3m}^b d}A_{6m}^b\right)\right\}\\
&+\sum_{n=0}^{\infty}\hat{\mu}_m^b\left\{\delta_{1n}^a\left(\mathrm{E}_{1nm}^{ab}A_{1n}^a+\mathrm{F}_{1nm}^{ab}A_{2n}^a\right)+\delta_{2n}^a\left(\mathrm{E}_{2nm}^{ab}A_{3n}^a+\mathrm{F}_{2nm}^{ab}A_{4n}^a\right)\right.\\
&\left.+\left(\frac{\hat{\mu}_n^{a2}}{\delta_{3n}^a}\right)\left(\mathrm{E}_{3nm}^{ab}A_{5n}^a+\mathrm{F}_{3nm}^{ab}A_{6n}^a\right)\right\}=0,\qquad m=1,2,3,\ldots
\end{aligned}\tag{43}$$

$$\begin{aligned}
&\delta_{1m}^b\left(e^{-\delta_{1m}^b d}A_{1m}^b-e^{\delta_{1m}^b d}A_{2m}^b\right)+\delta_{2m}^b\left(e^{-\delta_{2m}^b d}A_{3m}^b-e^{\delta_{2m}^b d}A_{4m}^b\right)\\
&+\left(\frac{\hat{\mu}_m^{b2}}{\delta_{3m}^b}\right)\left(e^{-\delta_{3m}^b d}A_{5m}^b-e^{\delta_{3m}^b d}A_{6m}^b\right)=0,\qquad m=0,1,2,\ldots
\end{aligned}\tag{44}$$

$$\begin{aligned}
&\frac{b}{2}\hat{\mu}_m^b\left\{2\delta_{1m}^b\left(A_{1m}^b-A_{2m}^b\right)+2\delta_{2m}^b\left(A_{3m}^b-A_{4m}^b\right)+\left(\delta_{3m}^b+\frac{\hat{\mu}_m^{b2}}{\delta_{3m}^b}\right)\left(A_{5m}^b-A_{6m}^b\right)\right\}\\
&+\sum_{n=0}^{\infty}\hat{\mu}_m^b\hat{\mu}_n^a\sin\hat{\mu}_n^a d\left\{2\delta_{1n}^a\left(\mathrm{E}_{1nm}^{ab}A_{1n}^a+\mathrm{F}_{1nm}^{ab}A_{2n}^a\right)+2\delta_{2n}^a\left(\mathrm{E}_{2nm}^{ab}A_{3n}^a+\mathrm{F}_{2nm}^{ab}A_{4n}^a\right)\right.\\
&\left.+\left(\delta_{3n}^a+\frac{\hat{\mu}_n^{a2}}{\delta_{3n}^a}\right)\left(\mathrm{E}_{3nm}^{ab}A_{5n}^a+\mathrm{F}_{3nm}^{ab}A_{6n}^a\right)\right\}=0,\qquad m=1,2,3,\ldots
\end{aligned}\tag{45}$$

$$\begin{aligned}&\frac{b}{2}\left(1+\delta_{0m}\right)\left\{\overline{\lambda}_{1m}^{b}\left(A_{1m}^{b}+A_{2m}^{b}\right)+\overline{\lambda}_{2m}^{b}\left(A_{3m}^{b}+A_{4m}^{b}\right)-2G\hat{\mu}_{m}^{b2}\left(A_{5m}^{b}+A_{6m}^{b}\right)\right\}\\&+\sum_{n=0}^{\infty}\cos\hat{\mu}_{n}^{a}d\left\{\lambda_{1n}^{a}\delta_{1n}^{a}\left(\mathrm{E}_{1nm}^{ab}\,A_{1n}^{a}+\mathrm{F}_{1nm}^{ab}\,A_{2n}^{a}\right)+\lambda_{2n}^{a}\delta_{2n}^{a}\left(\mathrm{E}_{2nm}^{ab}\,A_{3n}^{a}+\mathrm{F}_{2nm}^{ab}\,A_{4n}^{a}\right)\right.\\&\qquad\left.+2G\hat{\mu}_{n}^{a2}\delta_{3n}^{a}\left(\mathrm{E}_{3nm}^{ab}\,A_{5n}^{a}+\mathrm{F}_{3nm}^{ab}\,A_{6n}^{a}\right)\right\}=0\,,\qquad m=0,1,2,\ldots\end{aligned}\tag{46}$$

$$\begin{aligned}&\mathrm{S}_{m}^{a}\left\{\overline{\lambda}_{1m}^{a}\left(e^{-\delta_{1m}^{a}b}A_{1m}^{a}+A_{2m}^{a}\right)+\overline{\lambda}_{2m}^{a}\left(e^{-\delta_{2m}^{a}b}A_{3m}^{a}+A_{4m}^{a}\right)-2G\hat{\mu}_{m}^{a2}\left(e^{-\delta_{3m}^{a}b}A_{5m}^{a}+A_{6m}^{a}\right)\right\}\\&+\sum_{n=0}^{\infty}(-1)^{n}\left\{\lambda_{1n}^{b}\delta_{1n}^{b}\left(\mathrm{G}_{1nm}^{ba}\,A_{1n}^{b}-\mathrm{H}_{1nm}^{ba}\,A_{2n}^{b}\right)+\lambda_{2n}^{b}\delta_{2n}^{b}\left(\mathrm{G}_{2nm}^{ba}\,A_{3n}^{b}-\mathrm{H}_{2nm}^{ba}\,A_{4n}^{b}\right)\right.\\&\qquad\left.+2G\hat{\mu}_{n}^{b2}\delta_{3n}^{b}\left(\mathrm{G}_{3nm}^{ba}\,A_{5n}^{b}-\mathrm{H}_{3nm}^{ba}\,A_{6n}^{b}\right)\right\}=0\,,\qquad m=0,1,2,\ldots\end{aligned}\tag{47}$$

$$\begin{aligned}&\sum_{n=0}^{\infty}\mathrm{T}_{mn}^{a}\,\hat{\mu}_{n}^{a}\left\{2\delta_{1n}^{a}\left(e^{-\delta_{1n}^{a}b}A_{1n}^{a}-A_{2n}^{a}\right)+2\delta_{2n}^{a}\left(e^{-\delta_{2n}^{a}b}A_{3n}^{a}-A_{4n}^{a}\right)\right.\\&\qquad\left.+\left(\delta_{3n}^{a}+\frac{\hat{\mu}_{n}^{a2}}{\delta_{3n}^{a}}\right)\left(e^{-\delta_{3n}^{a}b}A_{5n}^{a}-A_{6n}^{a}\right)\right\}=0\,,\qquad m=0,1,2,\ldots\end{aligned}\tag{48}$$

$$\begin{aligned}&\mathrm{S}_{m}^{a}\left\{\overline{\lambda}_{1m}^{a}\left(A_{1m}^{a}+e^{-\delta_{1m}^{a}b}A_{2m}^{a}\right)+\overline{\lambda}_{2m}^{a}\left(A_{3m}^{a}+e^{-\delta_{2m}^{a}b}A_{4m}^{a}\right)-2G\hat{\mu}_{m}^{a2}\left(A_{5m}^{a}+e^{-\delta_{3m}^{a}b}A_{6m}^{a}\right)\right\}\\&+\sum_{n=0}^{\infty}\left\{\lambda_{1n}^{b}\delta_{1n}^{b}\left(\mathrm{G}_{1nm}^{ba}\,A_{1n}^{b}-\mathrm{H}_{1nm}^{ba}\,A_{2n}^{b}\right)+\lambda_{2n}^{b}\delta_{2n}^{b}\left(\mathrm{G}_{2nm}^{ba}\,A_{3n}^{b}-\mathrm{H}_{2nm}^{ba}\,A_{4n}^{b}\right)\right.\\&\qquad\left.+2G\hat{\mu}_{n}^{b2}\delta_{3n}^{b}\left(\mathrm{G}_{3nm}^{ba}\,A_{5n}^{b}-\mathrm{H}_{3nm}^{ba}\,A_{6n}^{b}\right)\right\}=0\,,\qquad m=0,1,2,\ldots\end{aligned}\tag{49}$$

$$\begin{aligned}&\sum_{n=0}^{\infty}\mathrm{T}_{mn}^{a}\,\hat{\mu}_{n}^{a}\left\{2\delta_{1n}^{a}\left(A_{1n}^{a}-e^{-\delta_{1n}^{a}b}A_{2n}^{a}\right)+2\delta_{2n}^{a}\left(A_{3n}^{a}-e^{-\delta_{2n}^{a}b}A_{4n}^{a}\right)\right.\\&\qquad\left.+\left(\delta_{3n}^{a}+\frac{\hat{\mu}_{n}^{a2}}{\delta_{3n}^{a}}\right)\left(A_{5n}^{a}-e^{-\delta_{3n}^{a}b}A_{6n}^{a}\right)\right\}=0\,,\qquad m=0,1,2,\ldots\end{aligned}\tag{50}$$

$$\begin{aligned}&\mathrm{S}_{m}^{a}\,\omega^{2}\rho_{w}\left(\frac{S+if_{p}}{n'}-1\right)\left\{\Lambda_{1m}^{a}\left(A_{1m}^{a}+e^{-\delta_{1m}^{a}b}A_{2m}^{a}\right)+\Lambda_{2m}^{a}\left(A_{3m}^{a}+e^{-\delta_{2m}^{a}b}A_{4m}^{a}\right)\right\}\\&+\sum_{n=0}^{\infty}\omega^{2}\rho_{w}\left(\frac{S+if_{p}}{n'}-1\right)\left\{\delta_{1n}^{b}\Lambda_{1n}^{b}\left(\mathrm{G}_{1nm}^{ba}\,A_{1n}^{b}-\mathrm{H}_{1nm}^{ba}\,A_{2n}^{b}\right)+\delta_{2n}^{b}\Lambda_{2n}^{b}\left(\mathrm{G}_{2nm}^{ba}\,A_{3n}^{b}-\mathrm{H}_{2nm}^{ba}\,A_{4n}^{b}\right)\right\}\\&+\sum_{n=0}^{\infty}i\omega\rho_{w}\mu_{n}\,\mathrm{K}_{nm}^{a}\,C_{n(I)}=-\rho_{w}gA_{I}\mu_{0}\frac{\mathrm{K}_{0m}^{a}}{\cos\mu_{0}d}\,,\qquad m=0,1,2,\ldots\end{aligned}\tag{51}$$

$$\begin{aligned}&\sum_{n=0}^{\infty}i\omega\mu_{m}\,\mathrm{K}_{mn}^{a}\left(1-\frac{n'}{S+if_{p}}\right)\left\{\delta_{1n}^{a}\left(1-\Lambda_{1n}^{a}\right)\left(A_{1n}^{a}-e^{-\delta_{1n}^{a}b}A_{2n}^{a}\right)+\delta_{2n}^{a}\left(1-\Lambda_{2n}^{a}\right)\left(A_{3n}^{a}-e^{-\delta_{2n}^{a}b}A_{4n}^{a}\right)\right.\\&\qquad\left.+\left(\frac{\hat{\mu}_{n}^{a2}}{\delta_{3n}^{a}}\right)\left(A_{5n}^{a}-e^{-\delta_{3n}^{a}b}A_{6n}^{a}\right)\right\}-\mu_{m}\,\mathrm{S}_{m}\,C_{m(I)}=\frac{igA_{I}\mu_{0}}{\omega}\frac{\delta_{0m}\,\mathrm{S}_{0}}{\cos\mu_{0}d}\,,\qquad m=0,1,2,\ldots\end{aligned}\tag{52}$$

$$\begin{aligned}
&\mathrm{S}_m^a \omega^2 \rho_w \left( \frac{S+if_p}{n'} - 1 \right) \left\{ \Lambda_{1m}^a \left( e^{-\delta_{1m}^a b} A_{1m}^a + A_{2m}^a \right) + \Lambda_{2m}^a \left( e^{-\delta_{2m}^a b} A_{3m}^a + A_{4m}^a \right) \right\} \\
&+ \sum_{n=0}^{\infty} (-1)^n \omega^2 \rho_w \left( \frac{S+if_p}{n'} - 1 \right) \left\{ \delta_{1n}^b \Lambda_{1n}^b \left( \mathrm{G}_{1nm}^{ba} A_{1n}^b - \mathrm{H}_{1nm}^{ba} A_{2n}^b \right) + \delta_{2n}^b \Lambda_{2n}^b \left( \mathrm{G}_{2nm}^{ba} A_{3n}^b - \mathrm{H}_{2nm}^{ba} A_{4n}^b \right) \right\} \\
&+ \sum_{n=0}^{\infty} i\omega \rho_w \mu_n \mathrm{K}_{nm}^a C_{n(II)} = 0 , \qquad m = 0, 1, 2, \ldots
\end{aligned} \tag{53}$$

$$\begin{aligned}
&\sum_{n=0}^{\infty} i\omega \mu_m \mathrm{K}_{mn}^a \left( 1 - \frac{n'}{S+if_p} \right) \left\{ \delta_{1n}^a \left( 1 - \Lambda_{1n}^a \right) \left( e^{-\delta_{1n}^a b} A_{1n}^a - A_{2n}^a \right) + \delta_{2n}^a \left( 1 - \Lambda_{2n}^a \right) \left( e^{-\delta_{2n}^a b} A_{3n}^a - A_{4n}^a \right) \right. \\
&\qquad \left. + \left( \frac{\hat{\mu}_n^{a2}}{\delta_{3n}^a} \right) \left( e^{-\delta_{3n}^a b} A_{5n}^a - A_{6n}^a \right) \right\} + \mu_m \mathrm{S}_m C_{m(II)} = 0 , \qquad m = 0, 1, 2, \ldots
\end{aligned} \tag{54}$$

and

$$\left.\begin{aligned} A_{50}^b &= 0 \\ A_{60}^b &= 0 \end{aligned}\right\} \tag{55}$$

in which

$$\mathrm{S}_m^a = \frac{d}{2} + \frac{\sin 2\hat{\mu}_m^a d}{4\hat{\mu}_m^a} \tag{56}$$

$$\mathrm{S}_m = \frac{d}{2} + \frac{\sin 2\mu_m d}{4\mu_m} \tag{57}$$

$$\mathrm{T}_{mn}^a = \begin{cases} \dfrac{d}{2} - \dfrac{\sin 2\hat{\mu}_m^a d}{4\hat{\mu}_m^a}, & m = n \\ \dfrac{g}{\omega^2} \dfrac{\sin 2\hat{\mu}_m^a d \, \sin 2\hat{\mu}_n^a d}{S+if_p}, & m \neq n \end{cases} \tag{58}$$

$$\mathrm{E}_{inm}^{ab} = \frac{1}{\hat{\mu}_m^{b\,2} + \delta_{in}^{a\,2}} \left[ 1 - (-1)^m e^{-\delta_{in}^a b} \right] \quad , \quad i = 1, 2, 3 \tag{59}$$

$$\mathrm{F}_{inm}^{ab} = \frac{1}{\hat{\mu}_m^{b\,2} + \delta_{in}^{a\,2}} \left[ (-1)^m - e^{-\delta_{in}^a b} \right] \quad , \quad i = 1, 2, 3 \tag{60}$$

$$\mathrm{G}_{inm}^{ba} = \frac{1}{\hat{\mu}_m^{a\,2} + \delta_{in}^{b\,2}} \left[ \cos \hat{\mu}_m^a d - e^{-\delta_{in}^b d} + \frac{\hat{\mu}_m^a}{\delta_{in}^b} \sin \hat{\mu}_m^a d \right], \quad i = 1, 2, 3 \tag{61}$$

$$\mathrm{H}_{inm}^{ba} = \frac{1}{\hat{\mu}_m^{a\,2} + \delta_{in}^{b\,2}} \left[ \cos \hat{\mu}_m^a d - e^{-\delta_{in}^b d} - \frac{\hat{\mu}_m^a}{\delta_{in}^b} \sin \hat{\mu}_m^a d \right], \quad i = 1, 2, 3 \tag{62}$$

$$\mathrm{K}_{nm}^a = \frac{1}{\hat{\mu}_m^{a\,2} - \mu_n^{\,2}} \left[ \cos \hat{\mu}_m^a d \sin \mu_n d - \frac{\hat{\mu}_m^a}{\mu_n} \sin \hat{\mu}_m^a d \cos \mu_n d \right] \tag{63}$$

$$\lambda_{\ell n}^{\psi} = \frac{2G}{1\text{-}2\mu}\left[(1-\mu)(\hat{\mu}_n^{\psi})^2 - \mu(\delta_{\ell n}^{\psi})^2\right], \quad \psi = a,b\,, \quad \ell = 1, 2 \tag{64}$$

$$\bar{\lambda}_{\ell n}^{\psi} = \frac{2G}{1\text{-}2\mu}\left[\mu(\hat{\mu}_n^{\psi})^2 - (1-\mu)(\delta_{\ell n}^{\psi})^2\right], \quad \psi = a,b\,, \quad \ell = 1, 2 \tag{65}$$

In the computations, if $N + 1$ wave components are adopted, a total of 14($N$+1) equations are obtained from Eqs. (41)-(55). As there are also 14($N + 1$) unknowns, $C_{n(I)}$, $C_{n(II)}$, $A_{1n}^{a} - A_{6n}^{a}$, and $A_{1n}^{b} - A_{6n}^{b}$ ( $n = 0, 1, 2, \ldots, N$ ), in these extended equations, $C_{n(I)}$, $C_{n(II)}$, $A_{1n}^{a} - A_{6n}^{a}$, and $A_{1n}^{b} - A_{6n}^{b}$ can be determined.

## REFERENCES


Augustin, L. N., J. L. Irish and P. Lynett (2009). Laboratory and numerical studies of wave damping by emergent and near emergent wetland vegetation. Coastal Engineering 56(3), 332-340.

Biot, M. A. (1956). Theory of propagation elastic waves in a fluid saturated porous solid. I. low-frequency range. The Journal of the Acoustical Society of America28(2), 168-178.

Chen, T. W., L. H. Huang and C. H. Song (1997). Dynamic response of poro-elastic bed to nonlinear water waves. Journal of Engineering Mechanics 123(10), 1041-1049.

Chou, C. R. and H. M. Fang (1995). Characteristic of wave dissipation due to the elastic membrane on water surface. Proc. 17th Conf. on Ocean Engineering in Taiwan, Taiwan, ROC, 443-458.

Gere, J. M. and S. P. Timoshenko (1984). Mechanics of Materials, 2nd ed., Boston, Mass.: PWS Engineering, 762 p.

Hsu, J. R. C., D. S. Jeng and C. P. Tsai (1993). Short-crested wave-induced soil response in a porous seabed of infinite thickness. International Journal for Numerical and Analytical Methods in Geomechanics 17, 553-576.

Jadhav, R. S., Q. Chen and J. M. Smith (2013). Spectral distribution of wave energy dissipation by salt marsh vegetation. Coastal Engineering 77, 99-107.

John, B. M., K. G. Shirlal and S. Rao (2015). Effect of artificial vegetation on wave attenuation – an experimental investigation. Procedia Engineering 116, 600-606.

Lan, Y. J. (2000). Analysis of Waves Interaction with Poro-elastic Structures, Ph. D. Thesis, National Cheng Kung University, Taiwan, ROC. (in Chinese)

Lan, Y. J., T. W. Hsu, F. X. Gan and C. Y. Li (2016). Mathematical study of wave interaction with a mound type of composite poro-elastic submerged breakwater. Ocean Engineering 124, 1-12.

Lan, Y. J., T. W. Hsu, J. W. Lai, C. C. Chang and C. H. Ting (2011). Bragg scattering of waves propagating over a series of poro-elastic submerged breakwaters. Wave Motion 48, 1-12.

Lan, Y. J., T. W. Hsu, and Y. R. Liu (2013). Analysis of wave interaction with an adjoining-type of composite poro-elastic submerged breakwater. Proc. 23rd Int. Offshore and Polar Eng., Anchorage, Alaska, USA, 1152-1159.

Lan, Y. J., Y. S. Kuo, T. W. Hsu and C. Y. Chen (2013). On waves propagating over two submerged closely spaced poro-elastic breakwaters. Proc. Inst. Mech. Eng. Part M: J. Eng. Marit. Environ. 227(3), 295-308.

Lan, Y. J. and J. F. Lee (2010). On Waves propagating over a submerged poro-elastic structure. Ocean Engineering 37, 705-717.

Lee, J. F. and C. J. Chen (1990). Wave Interaction with hinged flexible breakwater. Journal of Hydraulic Research 28 (3), 283-297.

Lee, J. F. and Y. J. Lan (1991). On effects of flexible circular cylinder to incident waves. Proc. 15th National Conf. on Theor. and Appl. Mech., Taiwan, ROC, 265-272.

Li, C. W. and K. Yan (2007). Numerical investigation of wavecurrent-vegetation interaction. Journal of Hydraulic Engineering 133(7), 794-803.

Liu, X. (2009). Seismic Wave Propagation and Modelling in Poro-Elastic Media with Mesoscopic Inhomogeneities. Ph.D. Thesis, The University of Adelaide, Australia.

Liu, X., S. Greenhalgh and Y. Wang (2011). 2.5-D poroelastic wave modelling in double porosity media. Geophysical Journal International 186(3), 1285-1294.

Mandal, S. and T. Sahoo (2014). Gravity wave interaction with porous and flexible cylinder system. Proceedings of the Fifth Indian National Conference on Harbour and Ocean Engineering, Goa, India, 1-6.

Mendez, F. and I. J. Losada (2004). An empirical model to estimate the propagation of random breaking and non-breaking waves over vegetation fields. Coastal Engineering 51(2), 103-118.

Möller, I., T. Spencer, J. R. French, D. J. Leggett and M. Dixon (1999). Wave transformation over salt marshes: a field and numerical modelling study from North Norfolk, England. Estuarine, Coastal and Shelf Science 49(3), 411-426.

Ohyama, T., M. Tanaka, T. Kiyokawa, T. Uda and Y. Murai (1989). Transmission and reflection characteristics of waves over a submerged flexible mound. Coastal Engineering in Japan 32(1), 53-68.

Sawaragi, T. (1995). Coastal Engineering – Waves, Beaches, Wave-Structure Interactions. Elsevier, Amsterdam, New York, 263-264.

Shanta, B. N. and T. Sahoo (2006). Wave interaction with a flexible porous breakwater in a two-layer fluid. Journal of Engineering Mechanics 132(9), 1007-1014.

Sollitt, C. K. and R. H. Cross (1972). Wave transmission through permeable breakwaters. Proc. 13th Coastal Engineering Conf., ASCE, Vancouver, 1827-1846.

Stratigaki, V., E. Manca, P. Prinos, I. Losada, J. L. Lara, M. Sclavo, C. L. Amos, I. Cáceres and A. Sánchez-Arcilla (2011). Large-scale experiments on wave propagation over posidonia oceanica. Journal of Hydraulic Research 49(S1), 31-43.

Tcheverda V., V. Kostin, G. Reshetova and V. Lisitsa (2017). Simulation of Seismic Waves Propagation in Multiscale Media. In: Voevodin V., Sobolev S. (eds) Supercomputing. RuSCDays 2017. Communications in Computer and Information Science 793. Springer, Cham.

Tong, L. H., Y. S. Liu, D. X. Geng, and S. K. Lai (2017). Nonlinear wave propagation in porous materials based on the Biot theory. The Journal of the Acoustical Society of America 142(2), 756-770.

Tseng, C. M., T. L. Tsai and L. H. Huang (2008). Effects of body force on transient poroelastic consolidation due to groundwater pumping. Environmental Geology 54, 1507-1516.

Wang, K. H. and X. Ren (1993). Water waves on flexible and porous breakwaters. Journal of Engineering Mechanics 119(5), 1025-1047.

Watarai, H., Y. Ohashi and S. Nagasaki (1987). Wave dissipating structure of new type using piles and flexible textile sheet. Proc. 34th Japanese Conf. on Coastal Engineering, JSCE, 502-506.

Xie P. Y. and D. H. Yang (2018). Seismic wave propagation model in near-surface strong-attenuation media. Chinese Journal of Geophysics 61(3), 917-925.

Yip, T. L., T. Sahoo and A. T. Chwang (2002). Trapping of surface waves by porous and flexible structures. Wave Motion 35, 41-54.

Zhang, Y., Y. Xu, J. Xia, P. Ping and S. Zhang (2014). On dispersive propagation of surface waves in patchy saturated porous media. Wave Motion 51, 1225-1236.